

PRIMERJAVA VSEBNOSTI VODNE PARE V STOLPCU ZRAKA NA PODLAGI RADIOSONDAŽE TER OPAZOVANJ GPS IN FOTOMETRA

INTERCOMPARISONS OF PRECIPITABLE WATER VAPOUR DERIVED FROM RADIOSONDE, GPS AND SUNPHOTOMETER OBSERVATIONS

Shaoqi Gong, Wenqin Chen, Cunjie Zhang, Ping Wu, Jing Han

UDK: UDK: 528.28
Klasifikacija prispevka po COBISS.SI: 1.01
Prispelo: 8. 5. 2020
Sprejeto: 1. 10. 2020

DOI: 10.15292/geodetski-vestnik.2020.04.562-577
SCIENTIFIC ARTICLE
Received: 8. 5. 2020
Accepted: 1. 10. 2020

IZVLEČEK

Atmosferska vsebnost vodne pare v stolpcu zraka PWV (angl. precipitable water vapor) je globalno izrednega pomena tako z vidika hidriološkega kroženja kot prenosa energije. Radiosonde, sončni fotometer in sprejemniki GPS (pa tudi širše GNSS) so postali temeljni instrumenti za terestrično opazovanje PVV. Pri študiji smo imeli na voljo vse tri instrumente, ki so bili hkrati nameščeni na opazovalnih postajah, ki so geografsko pokrivala tri tipične podnebne pasove. Podatke PWV z vseh instrumentov smo združili glede na čas opazovanj. Po tem, ko smo odstranili izstopajoča opazovanja, smo izvedli primerjavo vrednosti PWV za vsak par opazovanj različnih instrumentov. Ugotavljamo, da geografska širina in podnebje ne vplivata pomembneje na vrednosti PWV, pridobljene z radiosondažo, z opazovanji GPS ali opazovanji s fotometrom. Odstopanja v vrednostih PWV za katerikoli par instrumentov so normalno porazdeljena, kar pomeni, da v podatkih PWV ni sistematičnih pogreškov. Relativne razlike med vrednostmi PWV, pridobljenimi z radiosondažo in opazovanji GPS, so najmanjše, nekoliko večje so razlike med vrednostmi, pridobljenimi z radiosondažo in fotometrijo, največje razlike pa so med vrednostmi, pridobljenimi z opazovanji GPS in radiosondažo. Študija je zanimiva za spodbujanje uporabe sprejemnikov GPS (GNSS) in fotometrov za določanje vrednosti PWV namesto radiosondaže, saj takšna opazovanja omogočajo tudi visoko časovno ločljivost.

ABSTRACT

The atmospheric precipitable water vapour (PWV) plays a crucial role in the hydrological cycle and energy transfer on a global scale. Radiosonde (RS), sunphotometer (SP) and GPS (as well as broader GNSS) receivers have gradually been the principal instruments for ground-based PWV observation. This study first co-locates the observation stations configured the three instruments in the globe and in three typical latitudinal climatic regions respectively, then the PWV data from the three instruments are matched each other according to the observing times. After the outliers are removed from the matched data pairs, the PWV intercomparisons for any two instruments are performed. The results show that the PWV estimates from any two instruments have a good agreement with very high correlation coefficients. The latitude and climate have no significant influence on the PWV measurements from the three instruments, indicating that the instruments are very stable and depend on their performance. The PWV differences of any two instruments display the normal distribution, indicating non-systematic biases among the two PWV datasets. The relative differences between SP and GPS are the smallest, the middle between SP and RS, and those between GPS and RS are the largest. This study will be useful to promote GPS (GNSS) and SP PWV to be a substitute for RS PWV as a benchmark because of their high temporal resolutions.

KLJUČNE BESEDE

primerjava, vsebnost vodne pare v stolpcu zraka, fotometer, GPS, radiosondaža

KEY WORDS

Intercomparison, precipitable water vapour, sunphotometer, GPS, radiosonde

1 INTRODUCTION

The precipitable water vapour (PWV) is an important constituent in the atmosphere and plays a crucial role in the hydrological cycle and energy transfer on the global scale (Wang et al., 2007). With the atmospheric circulation, vertical transport, evaporation and condensation, the PWV can be formed clouds and precipitation to affect the evolution of the weather. Since the PWV absorbs solar and atmospheric infrared radiation and then releases latent heat, it is the most abundant and principal greenhouse gas in the atmosphere, which has a fundamental influence on the global climate change (Chou and Arking, 1981). Although the proportion of PWV in the atmosphere is very small, it shows a large spatial and temporal variability with values varying from less than 5 mm at the poles to about 50 mm near the equator (Mockler, 1995); thus accurate observation of water vapour is very significant to study hydrologic cycle, forecast regional weather and understand global climate because atmospheric PWV is one of the most important parameters in the numerical weather forecasting models and climate models (Gulstad and Isaksen, 2007).

As for the PWV measurement, there are three kinds of data sources: (1) the reanalysis PWV data by the grid-based numerical forecasting model, such as European Center for Medium-Range Weather Forecasts (ECMWF), National Centers for Environmental Prediction (NCEP) and National Center for Atmospheric Research (NCAR) (Dee et al., 2011; Robert et al., 2001); (2) space-based PWV data retrieved from satellite near-infrared and thermal infrared images, and GNSS radio occultation; (3) the ground-based measurements by portable instruments, such as radiosonde (Zhai and Eskridge, 1997), Sunphotometer (Halthore et al., 1997), Global Navigation Satellite Systems (GNSS) (Lu et al., 2016), microwave radiometer (Liu et al., 2009) and Raman lidar (Wang et al., 2015). The reanalysis data can provide global water vapour data, but the spatial resolution is rather low. The space-based water vapour data have high spatial resolutions and are used widely in the weather and climate research. However, the accuracies of remotely sensed water vapour data still need to be validated by ground observation data.

A radiosonde is the earliest instrument for observing atmospheric profile parameters, and the radiosonde data have been regarded as a benchmark to evaluate and calibrate satellite remotely sensed observations (Kuo et al., 2005). Liu et al. used radiosonde PWV data from 83 sites in China to validate MODIS PWV products in the near-infrared and thermal infrared channels (Liu et al., 2015). Zeng et al. assessed the accuracy of AIRS water vapour mixing ratio and PWV products against radiosonde soundings from 113 sites across China (Zeng et al., 2019). As GPS meteorology was established to determine information on the state of the atmosphere, Bevis et al. first presented an approach to retrieve atmospheric PWV from the ground-based GPS (Bevis et al., 1992). Ground-based GPS is independent of meteorological events and is able to provide PWV estimates with high accuracy and temporal resolution (a 5-min sampling frequency). At present the International GNSS Service (IGS) can provide the GNSS product data such as zenith hydrostatic delay (ZPD) at about 400 stations worldwide (UCSD, 2002), then ZPD can be calculated to PWV content by combining with the surface pressure and temperature data. Vaquero-Martinez et al. validated the water vapour products from multi-sensors including MODIS, GOME-2, OMI, SEVIRI and SCIAMACHY using ground-based GPS PWV data in the Iberian Peninsula as a benchmark (Vaquero-Martínez et al., 2017, 2018). Alraddawi et al. assessed the quality of three satellite PWV datasets from MODIS, AIRS and SCIAMACHY against ground-based GNSS water vapour data at three reference Arctic observation sites (Alraddawi et al., 2018). Sunphotometer is

easily deployed in the field campaigns to estimate aerosol optical depth (AOD) and column abundance of water vapour from direct sun measurements in the visible and near-infrared channels; they have been increasingly used in the validation of satellite retrievals and radiometric calibration of the satellite remote sensor (Zibordi et al., 2009; Soe et al., 2014). Sun photometer CE-318, which is made by the CIMEL Electronique company in France, has become the principal instrument on the Aerosol Robotic Network (AERONET). AERONET provides a continuous, long term and readily accessible datasets of spectral AOD and precipitable water vapour at more than 1000 stations in the globe (Holben et al., 1998). Shi et al. used sunphotometer PWV data from AERONET as a benchmark to validate the PWV products from TERRA/MODIS, FY-3C/VIRR and MERSI over the typical regions in China (Shi et al., 2018). Vijayakumar et al. validated the AOD and PWV data from MODIS images and ECMWF model during 2005-2015 with ground-based sunphotometer observations from AERONET over Pune, India (Vijayakumar et al., 2018). Nowadays, radiosonde, GPS receiver and sunphotometer have become the principal ground-based instruments and are used widely in the meteorological observation and climatological research, however, their relative accuracies of three instruments are rarely compared on a global scale. The main purpose of this research is to conduct a comprehensive intercomparison of PWV data derived from the measurements of the three instruments, which will be useful to promote ground-based GNSS and sunphotometer PWV to be a substitute for radiosonde PWV as a benchmark because of their high temporal resolutions.

The remainder of this paper is organized as follows: Section 2 presents the descriptions of PWV data from radiosonde, GPS and sunphotometer and the preprocessing methods; Section 3 discusses the relative differences of three instruments by the PWV intercomparisons in the globe and in the different latitudes respectively; Section 4 offers the summary and conclusions.

2 DATA AND METHODS

2.1 PWV data retrieved from the three instruments measurements

2.1.1 Radiosonde PWV data

Since the global radiosonde network was established in the early 1940s, radiosondes have been the principal instruments used for observing the upper atmosphere. There are over 1000 radiosonde sites distributed worldwide (Ware et al., 1996; Wang et al., 2005). The radiosonde balloons are launched twice a day at zero and twelve o'clock GMT to observe the atmospheric profiles at these stations. The observations include geopotential height, air temperature, air pressure, relative humidity, wind direction and wind speed at standard levels, including the surface and the atmospheric levels of 1000, 925, 850, 700, 500, 400, 300, 250, 200, 150 and 100 hPa. The column integrated amount of atmospheric PWV is calculated by the integral of average specific humidity from the ground to the upper atmosphere at 300 hPa. It is expressed as the following equation (Wang and Liu, 1993):

$$PWV = \frac{1}{g\rho} \int_{p_0}^p q(p) dp = \frac{1}{g\rho} \sum_{i=1}^n q_i \Delta p \quad (1)$$

where g is the acceleration due to gravity for 980 cm/s^2 ; the water density ρ is given as 1 g/cm^3 ; p_0 and p are the respective air pressures in the surface and top of the atmosphere, and Δp is the pressure differ-

ence between the upper and lower atmospheric layers; n is the number of atmospheric layers from the ground to the top of atmosphere; q_i is the mean specific humidity corresponding to atmospheric layer i , and it is given as equation (2):

$$q = \frac{662e}{p - 0.378e} \tag{2}$$

here e is the water vapour partial pressure in the unit of hPa, which is computed by the dew point temperature using the saturation vapour pressure (e_w) formulation. The formulation is proposed by the World Meteorological Organization, as shown in equation (3):

$$e_w = 6.11 \exp\left(\frac{17.62T}{T + 243.12}\right) \tag{3}$$

Here T is air temperature or dew point temperature in Celsius degree ($^{\circ}\text{C}$) (WMO, 2008). The radiosonde data are available from the Meteorological Observatory at Nanjing University of Information Science and Technology (NUIST), China.

2.1.2 GPS PWV data

The American GPS is the earliest and most widely used Global Navigation Satellite System, and it has good accuracy for positioning, navigation and timing (Natraš et al., 2019). The GPS system is composed of a constellation of 30 operational satellites at 20200 km above the Earth, and these satellites are distributed evenly in 6 orbital planes with 55° inclination, and the travelling period of each satellite is 12 sidereal hours (Wang et al., 2007), which makes sure the radio signals from more than four satellites to be transmitted at anywhere on the globe at any time. Due to the refraction of atmospheric molecules and water vapour, the radio signals from the GPS satellites to ground receivers will propagate through the troposphere and are always delayed. The total tropospheric delay along the zenith path (called as zenith path delay, ZPD) can be divided into two parts: a hydrostatic term (ZHD) affected by dry gases and a wet term (ZWD) caused by water vapour (Shi et al., 2015). The ZPD can be calculated from GPS measurements using mapping functions, and the ZHD is computed as a function of the elevation H , latitude ϕ , and surface pressure P_s the by a model as Equation (4) (Elgered et al., 1991),

$$ZHD = \frac{(2.2779 \pm 0.0024)P_s}{1 - 0.00266(2\phi) - 0.00028H} \tag{4}$$

Then the ZWD is obtained by the subtraction of ZHD from ZPD. The PWV amount is calculated by a proportional constant Π as Equation (5) and (6) (Bevis et al., 1992),

$$PWV = \Pi \cdot ZWD \tag{5}$$

$$\Pi = \frac{10^5}{(k_2' + \frac{k_3}{T_m})\rho R_v} \tag{6}$$

where $k_2' = (17 \pm 10)$ K/hPa and $k_3 = 3.776 \times 10^5$ K²/hPa are the constants for the refractive index of the atmosphere (Bevis et al., 1994; Iwabuchi, Naito and Mannoji, 2000; Jade et al., 2005; Senica et al., 2018); ρ is the water density; R_v is the specific gas constant for water vapour; and the atmospheric

water-vapour-weighted mean temperature T_m is approximately calculated by the air temperature T_0 on the ground as $T_m = 0.72T_0 + 70.2$ (Bevis et al., 1992). The ZPD, air temperature and air pressure on the ground, including in the meteorological files of GPS Receiver Independent Exchange (RINEX), are available from the Scripps Orbit and Permanent Array Center (SOPAC) (<ftp://cddis.gsfc.nasa.gov/>).

2.1.3 Sunphotometer PWV data

Sun photometer CE-318, commercially manufactured by the CIMEL Electronique company in France, has been used quite widely in the globe and is the principal instrument on the AERONET. It can automatically track and point to the sun by a motor with two microprocessors, and the microprocessor calculates accurately solar zenith and azimuth angle from the date and time and the geographical coordinates of the instrument. The instrument has an optical header with two collimators for observing the sun and the sky respectively, so it can measure direct solar irradiance, the almucantar irradiance and the principal plane irradiance from the skylight on the ground (Campmany et al., 2010). The optical header has eight filters to measure the irradiance at 1020 nm, 936 nm, 870 nm, 675 nm, 500 nm, 440 nm, 380 nm and 340 nm. The AOD and PWV can be derived from the direct solar irradiance while irradiances from skylight are retrieved to size distribution parameters and phase function of aerosol. AERONET provides globally distributed AOD, PWV and inversion products following the standard processing algorithm. These products are classified into three data quality levels: the unscreened for level 1.0, the cloud-screened and quality controlled for level 1.5, and the quality-assured for level 2.0 (Giles et al., 2019). The sunphotometer PWV data in the research are the level 2.0 of AERONET, which are downloaded on the source website at <http://aeronet.gsfc.nasa.gov/>.

The retrieved PWV from sunphotometer is based on a couple of solar direct radiometric observations in near-infrared channels at 1020 nm and 936 nm, which the 936 nm is a strong absorption channel of water vapour, whereas the 1020 nm is only impacted by the aerosol scattering. Regarding the absorption channel at 936nm, an equation is given as the following form according to the Beer-Bouguer-Lambert law (Liou, 2002):

$$V_1/V_0 = \exp[-\tau_{a1}m - k(mW)^b] \quad (7)$$

where V_0 and V_1 are respectively the extraterrestrial value and the measurement from sunphotometer at 936nm, τ_{a1} is the aerosol scattering optical depth at 936 nm, the optical air mass m can be calculated with solar zenith angle θ_0 , W is the PWV amount, and b and k are the coefficients for the optical filter of the instrument at 936nm and are generally determined by the manufacturer depending on the instrument characteristics. When both sides of equation (7) are taken the natural logs, it is transformed into equation (8):

$$\ln(V_1) + \tau_{a1}m = \ln(V_0) - k(mW)^b \quad (8)$$

In order to calculate the water vapour amount, the scattering AOD at 936 nm (τ_{a1}) is necessary. And the AOD at 1020 nm (τ_{a2}) is derived firstly from solar direct radiometric observations of the instrument. Because of a good adjacency between the two channels at 1020 nm and 936 nm, a linear relationship between τ_{a2} and τ_{a1} can be deduced for the standard atmosphere from a radiative transfer model, that is $\tau_{a1} = 1.16\tau_{a2}$ (Morys et al., 2001). Therefore, the PWV amount W is expressed as the following equation:

$$\left[\frac{\ln(V_0) - \ln(V_1) - 1.16m}{km} \cdot a_2 \right]^{1/2} \tag{9}$$

2.2 Co-location of PWV data from three instruments

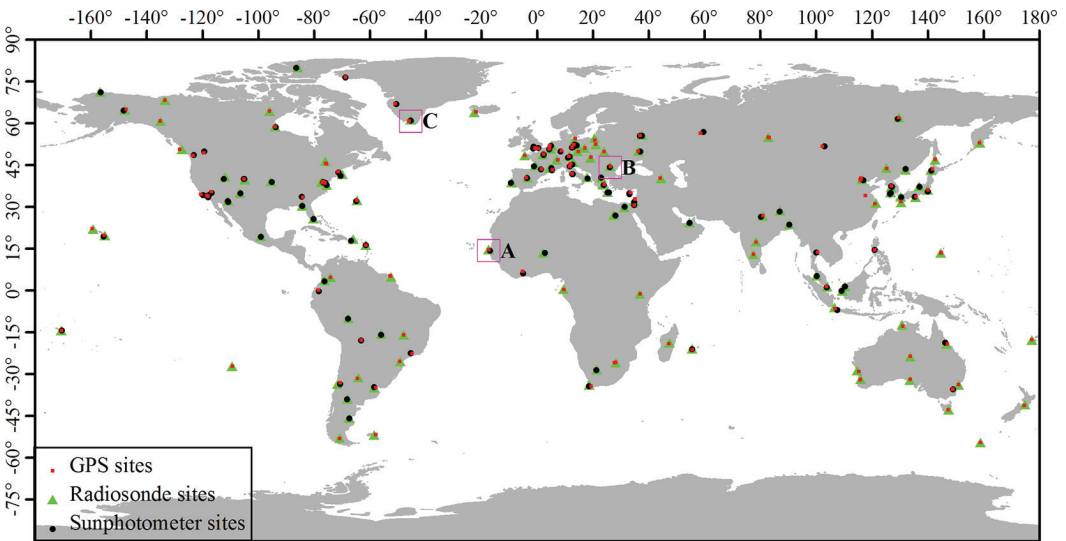


Figure 1: Co-located sites distribution map of three PWV instruments.

In order to inter-compare the relative differences of PWV data from the three ground-based instruments (radiosonde, GPS and sunphotometer), the observation positions and times for any two instruments must be matched. Since the observation station is dispersed for each instrument, the positions for any two instruments are co-located within 100 km referenced the previous studies (Dee et al., 2011; Smirnov et al., 2009; Xu, Luo, and Shi, 2009; Gong, 2018). The co-location procedure consists of the following steps and is implemented in the Geographic Information System software ArcGIS 10.5. Firstly, the station vector files for radiosonde, GPS and sunphotometer are respectively generated by the longitude and latitude data of all the stations worldwide. Secondly, all the stations of any two instruments are carried out the co-location. Taking instrument A and instrument B as an example, a circular buffer area with a radius of 100 km around each station of instrument B is created from its station vector file, and the station vector file of instrument A is clipped by the buffer file of instrument B so that the matched stations of instrument A are located in the buffer area of instrument B, then the clipped station vector file of instrument A is overlaid over the buffer file of instrument B using an intersection operation, which the spatial attributes of stations for the instrument A and B are joined and achieve the co-location of all the stations for the two instruments. Hence, the number of co-located stations is 126 for radiosonde, 128 for GPS and 124 for sunphotometer in the globe (Figure 1). Finally, the observation times of PWV data from any two instruments are matched. Since radiosonde observes the atmospheric profiles twice a day at zero and twelve o'clock GMT, GPS receiver obtains radio signal every 5 minutes, and sunphotometer points to the sun and measures the irradiances every 15 minutes, hence the time difference of the matched PWV data is ±5 minutes between radiosonde and GPS, ±15 minutes between radiosonde and sunphotometer and ±5 minutes between GPS and sunphotometer. All the PWV data from the three instruments are

collected from January to December 2017. Due to the stochastic errors in the measurements from the three instruments, there are some outliers among the matched PWV data pairs. All PWV differences between any two instruments twice higher than the standard deviation are regarded as outliers and are eliminated (Li, Muller and Cross, 2003; Birkenheuer and Gutman, 2005).

3 RESULTS AND DISCUSSION

3.1 Intercomparisons of PWV from three instruments in the globe

In order to determine the relative differences of PWV data from the three instruments, the multiple PWV comparisons for any two instruments are carried out for all co-located stations in the globe. The PWV scatter plot between two instruments is drawn, and the correlation coefficient (R), the root mean square difference (RMS), the mean bias (MB), the slope and intercept of the least-square regression line are computed. Furthermore, the frequency distribution histogram of PWV difference between two instruments is plotted, the difference statistics including frequency, mean, standard deviation (sd), skewness and kurtosis are calculated. Hence, the relative difference between any two instruments is evaluated by these statistical indices.

3.1.1 Comparisons of PWV between radiosonde and GPS in the globe

Figure 2a is the PWV scatter plot between GPS and radiosonde, the number of the matched data pairs is 13705, and the points are located near the 1:1 line in the scatter plot. This shows that GPS PWV data are in a very good agreement with the radiosonde ones, and their correlation coefficient is very high for 0.968. The mean bias of GPS PWV data relative to radiosonde ones is very large for -5.29 mm, indicating GPS PWV data are lower than radiosonde ones. And it is evident that most of the points are distributed on the right side of the 1:1 line in figure 2a. The least-square regression indicates that GPS PWV data is 0.903 times higher than radiosonde ones, with a zero-point offset of -2.669 mm. The slope (<1) and offset (<0) of the regression line implies a systematic underestimation for all the GPS PWV data. The RMS of GPS PWV data against radiosonde ones is 7.05 mm, which is much larger than the results about 1-3 mm by previous studies (Lu et al., 2016; Duan et al., 1996; Deblonde et al., 2005). For example, Tregoning et al. evaluated the absolute accuracy of GPS-derived PWV at Cape Grim, Tasmania during November and December 1995 and showed that the root mean square difference between GPS and radiosonde PWV was 1.5 mm (Tregoning et al., 1998). Ohtani and Naito investigated the accuracy of PWV obtained from the Japanese Global Positioning System network and indicated that the GPS PWV was 3.7 mm in term of root mean square difference and a mean bias of -2.7 mm compared with radiosonde observations (Ohtani and Naito, 2000). The large relative difference between GPS and radiosonde PWV data in this study is probably in connection with the comparison on a global scale, whereas the previous results are from the local regions. Since atmospheric water vapour varies quickly as space and season changed, the PWV measurements from ground-based instruments are often influenced by many factors, such as undersampling in the upper atmosphere, sensor freezing and subsequent latent heat release of atmosphere, and different time lags between wet and dry bulb temperature measurements for radiosonde (Bruegge et al., 1992; Campmany et al., 2010); GPS satellite orbits, elevation cutoff angle, mapping function, network configuration, surface air pressure and the atmospheric weighted-mean-temperature

for GPS-derived PWV (Tregoning et al., 1998; Wang et al., 2007), which results in the large difference between radiosonde and GPS worldwide. Furthermore, the observation paths of the two instruments are different. The balloon has a shift during ascent and the path of the radiosonde is declined and prolonged, whereas the path of radio signals is straight from GPS satellite to the tangent point on Earth. Hence, the column integrated amounts of PWV measured by the two instruments display rather different. Figure 2b is the frequency distribution histogram of PWV difference between radiosonde and GPS; the mean difference is -5.29 mm and the frequency is highest about 10% at this value, which approximates 1371 pairs of the matched PWV data. The standard deviation of PWV difference is 4.66 mm, meaning the most of differences within the range of -9.95 to -0.63 mm. Generally, the kurtosis and skewness of the standard normal distribution are 3 and 0, respectively. Here, the difference skewness is -0.56, indicating that the number of samples located in the left of the mean is a little larger than that of the right, but it is close to 0 for the standard normal distribution. The difference kurtosis, 2.80, approaches 3 for the normal distribution. Hence, the PWV difference histogram between GPS and radiosonde shows the normal distribution features, which suggests non-systematic bias among the two datasets.

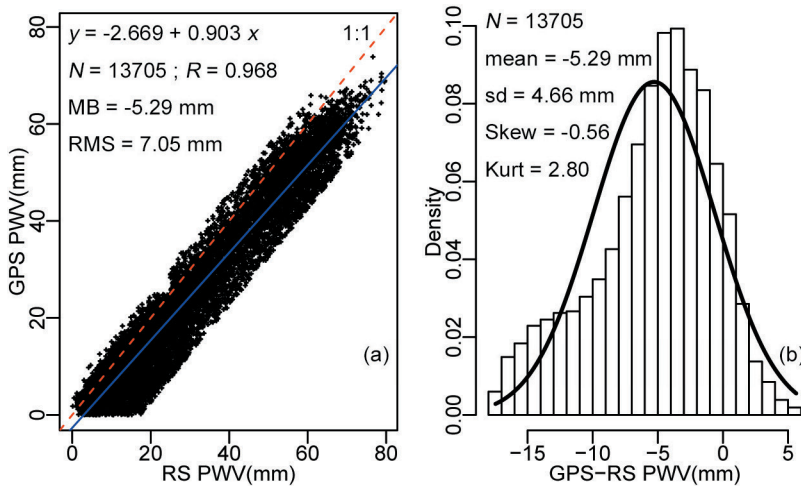


Figure 2: Comparison of the PWV from Radiosonde (RS) and GPS.

3.1.2 Comparisons of PWV between radiosonde and sunphotometer in the globe

Figure 3a is the PWV scatter plot between sunphotometer and radiosonde. Since sunphotometer works in the sunny and non-cloudy days, the number of the matched data pairs is relatively less for 3231, and the points are distributed around the 1:1 line in the scatter plot. This shows that sunphotometer PWV data agree well with the radiosonde ones, and a high correlation coefficient of 0.973 is observed between the two datasets. The least-square regression indicates that sunphotometer PWV data is 0.834 times higher than radiosonde ones, with an offset of 0.659 mm. The slope (<1) and offset (>0) of the regression line suggests a slight overestimation of sunphotometer PWV for low PWV amount and a slight underestimation for high PWV amount relative to radiosonde ones. The mean bias of sunphotometer PWV data in contrast to radiosonde ones is -2.22 mm, indicating that sunphotometer PWV data are a little lower than radiosonde ones, and the RMS of the two PWV datasets is 3.74 mm. Although the differences are

lower than those between GPS and radiosonde PWV data, they are higher than the previous results in local regions. For example, Campmany et al. compared the PWV measurements from sunphotometer and radiosonde during 2001-04 in Barcelona, Spain with the absolute difference of -2.62 mm and the RMSE of 1.76mm (Campmany et al., 2010). Halthore et al. suggested that the sunphotometer tended to underestimate an average of 10% PWV amount by the comparison with radiosonde data at Wallops Island, Virginia, in July 1993 (Halthore et al., 1997). The PWV retrieval uncertainty from sunphotometer observations is mainly attributed to the ageing effect of the filters, affecting the values of parameters k and b in equation (9). While cloud screening is incomplete, sunphotometer can underestimate the PWV amount. Similarly, the observation paths of the two instruments are also different, sunphotometer always points to the sun from ground during measuring, whereas the PWV integration from radiosonde data is never along the same line of sight as the measurement, which results in the large PWV difference between the two instruments. Figure 3b is the frequency distribution histogram of PWV difference between sunphotometer and radiosonde; the mean difference is -2.22 mm, and the highest frequency is about 15% at this value. The standard deviation of PWV difference is 3.01 mm, which implies the main differences ranging from -5.23 to 0.79 mm. The skewness and kurtosis of PWV difference are -0.39 and 2.88 respectively, approaching the thresholds of the standard normal distribution, which indicates that the PWV difference histogram between sunphotometer and radiosonde displays the normal distribution features and that there are no systematic biases among the two datasets.

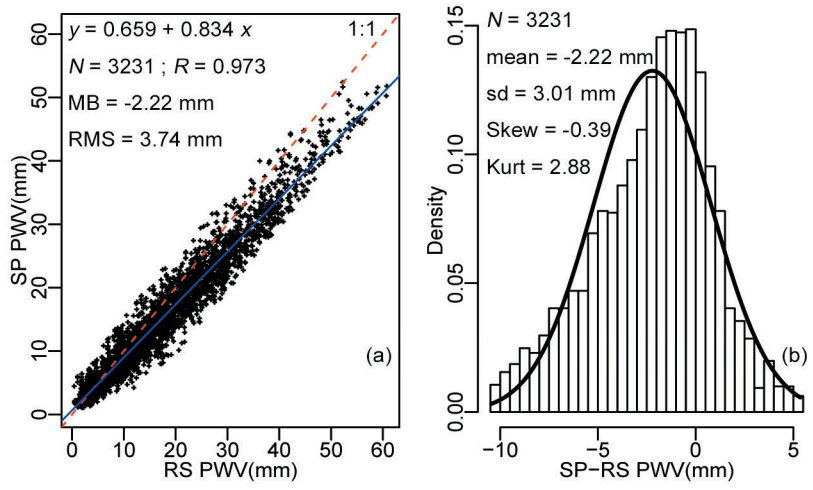


Figure 3: Comparison of PWV from Radiosonde (RS) and Sunphotometer (SP).

3.1.3 Comparisons of PWV between GPS and sunphotometer in the globe

Figure 4a is the PWV scatter plot between sunphotometer and GPS. Due to high sampling frequency of the two instruments with a 15-min period for sunphotometer and a 5-min period for GPS receiver, the number of the matched data pairs is the most for 138452 among the three comparisons, and the points are distributed on both sides of the 1:1 line in the scatter plot. This indicates that sunphotometer PWV data are very agreeable with the GPS ones, and a correlation coefficient of 0.959 is between the two datasets. The least-square regression concludes that sunphotometer PWV data is 0.879 times higher than GPS ones, with

an offset of 3.794 mm. The slope (<1) and offset (>0) of the regression line reveals a slight overestimation of sunphotometer PWV for low PWV amount and a slight underestimation for high PWV amount in contrast to GPS ones. The mean bias of sunphotometer PWV data against GPS ones is 1.84 mm, showing that sunphotometer PWV data are higher than GPS ones, and the RMS of the two PWV datasets is 3.65 mm. The mean bias and RMS are the lowest among the three comparisons, which is similar to the previous results. For example, Bokoye et al. compared sunphotometer derived PWV to GPS PWV at four Canadian sites during the period 2000-04 and showed the RMS of 1.4-4.8 mm and the mean bias of -4.1-1.2 mm (Bokoye et al., 2007). Figure 4b is the frequency distribution histogram of PWV difference between sunphotometer and GPS; the mean difference is 1.84 mm, and the highest frequency is about 14% at this value. The standard deviation of PWV difference is 3.50 mm, which suggests the main differences within the range of -1.66 to 5.34 mm. The difference skewness is 0.19, indicating that the number of samples distributed in the left of the mean is a little less than that of the right, and the difference kurtosis is 3.33. The skewness and kurtosis of PWV difference are very close to the thresholds of the standard normal distribution, indicating that the PWV difference histogram between sunphotometer and GPS displays the normal distribution features and that there are no systematic biases among the two datasets.

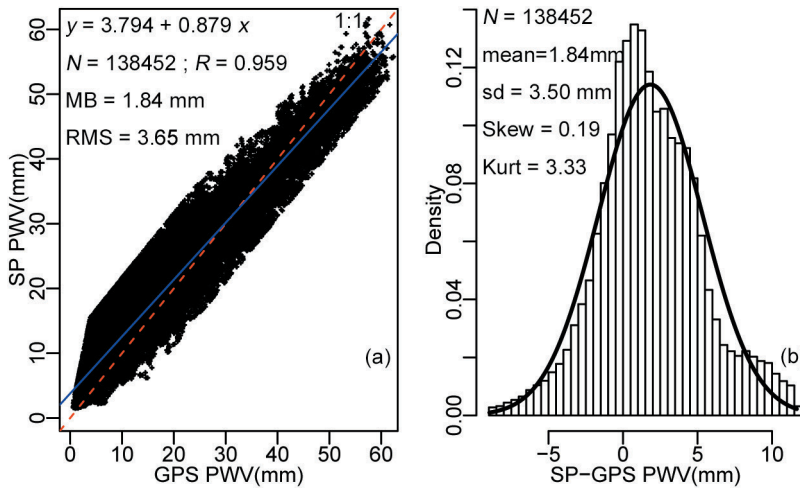


Figure 4: Comparison of the PWV from Sunphotometer (SP) and GPS.

3.2 Intercomparisons of PWV from three instruments in different latitudes

In order to determine the relative differences of PWV data from three individual instruments in different latitudes, the co-located stations in three typical climatic regions, including tropic, mid-latitude and sub-Arctic are selected in the study. The positions of the co-located stations are located respectively in area A, B and C in figure 1, and the detailed information of the co-located sites is listed Table 1. The height difference of the co-located sites is below 100 m for eliminating the influence of elevation on GPS-derived PWV. When the multiple PWV comparisons for any two instruments in different latitudes are performed, the time series charts of PWV data from any two instruments during the whole year in 2017 are drawn, and the correlation coefficient, mean bias and RMS are calculated in Table 2. Then relative differences between any two instruments in different latitudes are assessed by these statistical indices.

Table 1: Typical station of three instruments in three latitudinal regions.

	RS station				GPS station				SP station			
	No.	Lat(°)	Lon(°)	H(m)	Name	Lat(°)	Lon(°)	H(m)	Name	Lat(°)	Lon(°)	H(m)
Tropic	61641	14.73	-17.49	24	dakr	14.72	-17.44	51	Dakar	14.39	-16.96	4
Mid-Latitude	15420	44.50	26.13	91	bucu	44.46	26.13	113.2	Magurele_Inoc	44.35	26.03	19
Sub-Arctic	04270	61.18	-45.21	26	qaq1	60.72	-46.05	110.4	Narsarsuaq	61.16	-45.42	11

Table 2: Summary of intercomparison between radiosonde, GPS and sunphotometer PWV in three latitudinal regions.

	RS & GPS				RS & SP				SP & GPS			
	N	Bias	RMS	R	N	Bias	RMS	R	N	Bias	RMS	R
Tropic	278	-5.61	6.24	0.955	109	-4.43	5.45	0.937	11256	0.96	2.91	0.972
Mid-Latitude	551	-7.54	7.85	0.978	112	-3.23	4.12	0.982	12507	3.83	4.06	0.989
Sub-Arctic	452	-4.27	4.65	0.942	19	-1.41	1.56	0.986	3525	3.22	3.49	0.915

3.2.1 Comparisons of PWV between radiosonde and GPS in different latitudes

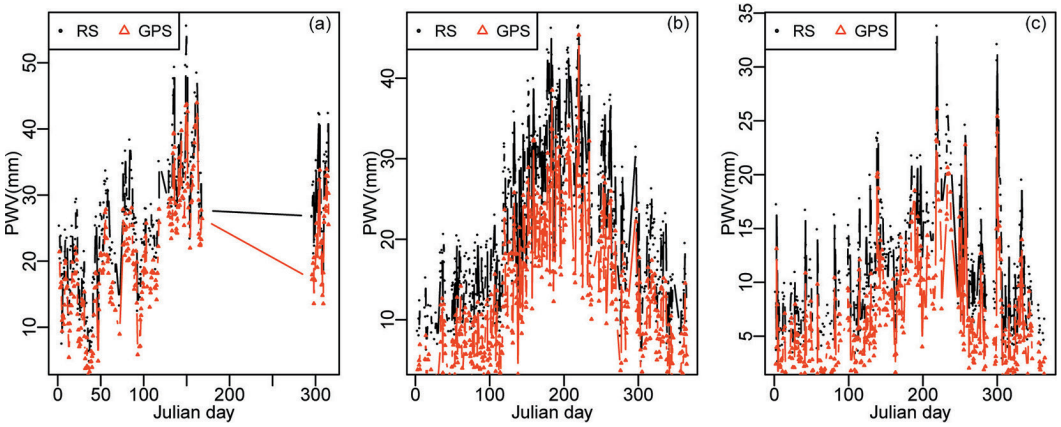


Figure 5: Time series chart of PWV from Radiosonde and GPS in three latitudinal regions: (a) Tropic, (b) Mid-Latitude and (c) Sub-Arctic.

Figure 5 is the time series charts of radiosonde and GPS PWV data at co-located stations in three latitudinal regions, the maximum PWV amount measured by the two instruments is in descending order from Tropic to Mid-latitude and then to Sub-Arctic. The individual GPS PWV point is always under the radiosonde PWV point in the chart, indicating that GPS PWV amounts are lower than radiosonde ones in different latitudes. Among the matched PWV data between radiosonde and GPS during the whole year in 2017, because the radiosonde PWV data from June 18 to October 22 are missed in the Tropic, the number of the matched data pairs is 278 from Table 2. The PWV data from the two instruments are very agreeable, with a high correlation coefficient of 0.955. The mean bias of GPS PWV relative to radiosonde PWV is -5.61 mm, and the RMS is 6.24 mm. The number of the matched data pairs in the Mid-latitude is 551, the two PWV datasets have a good relationship with a correlation coefficient of 0.978, and the mean bias and RMS are -7.54 mm and 7.85 mm respectively. The relative differences in the Mid-latitude are the largest in the three climatic regions. The number of the matched data pairs in

the Sub-Arctic is 452, the correlation coefficient of the two PWV datasets is 0.942, indicating that they agree well. The mean bias and RMS are the lowest in the three climatic regions, and they are -4.27mm and 4.65mm, respectively. In general, although GPS PWV data are in a very good agreement with the radiosonde ones in different latitudes and high correlation coefficients are between 0.942 and 0.978, the relative differences of PWV data between two individual instruments are rather higher, which the mean bias ranges from -4.27 mm to -7.54 mm and the RMS is within the range of 4.65 to 7.85 mm. This is probably due to the overestimation of radiosonde and the underestimation of GPS.

3.2.2 Comparisons of PWV between radiosonde and sunphotometer in different latitudes

Figure 6 is the time series charts of radiosonde and sunphotometer PWV data at co-located stations in three latitudinal regions; it is easy to be found that sunphotometer PWV amounts are also lower than radiosonde ones in different latitudes. Since radiosonde observes the atmospheric profiles only twice a day, the number of the matched data pairs for the individual instrument in different latitudes is few, but the PWV data from the two instruments agree well with high correlation coefficients from 0.937 to 0.986. Seen from Table 2, the number of the matched data pairs in the Tropic is 109; the mean bias is -4.43 mm and the RMS is 5.45 mm, which are largest relative differences in the three climatic regions. The number of the matched data pairs in the Mid-latitude is 112, and the relative differences are the middle with the mean bias of -3.23 mm and the RMS of 4.12 mm. The number of the matched data pairs in the Sub-Arctic is least for 19, the relative differences are the smallest, and the mean bias and the RMS are -1.41 mm and 1.56 mm respectively. The high relative differences between the two instruments probably result from the overestimation of radiosonde, especially in low and middle latitudes.

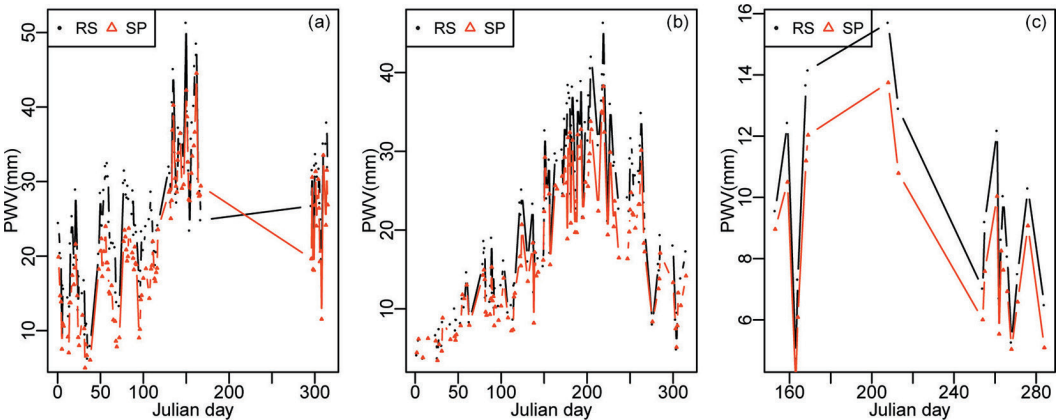


Figure 6: Time series chart of PWV from Radiosonde and Sunphotometer in three latitudinal regions: (a) Tropic, (b) Mid-Latitude and (c) Sub-Arctic.

3.2.3 Comparisons of PWV between GPS and sunphotometer in different latitudes

Figure 7 is the time series charts of sunphotometer and GPS PWV data at co-located stations in three latitudinal regions, the individual sunphotometer PWV point is always above the GPS PWV point in the chart, indicating that sunphotometer PWV amounts are higher than GPS ones in different latitudes. Since the sampling frequencies of sunphotometer and GPS receiver are very high, the numbers of the

matched data pairs in different latitudes are relatively large. The correlation coefficients of PWV data from the two individual instruments in different latitudes are very high and range from 0.915 to 0.989. This shows that the two instruments in different climatic regions have a good agreement for the measurements. Seen from Table 2, the number of the matched data pairs in the Tropic is 11256, the relative differences of the two instruments are the smallest in the three climatic regions, and the mean bias and the RMS are 0.96 mm and 2.91 mm respectively. The number of the matched data pairs in the Mid-latitude is 12507, the mean bias is 3.83 mm, and the RMS is 4.06 mm, which are the largest relative differences. Since sunphotometer, PWV data from January 1 to May 30 are missed in the Sub-Arctic, the number of the matched data pairs is least for 3525, and the relative differences are the middle with the mean bias of 3.22 mm and the RMS of 3.49 mm. The relative differences between sunphotometer and GPS are the least among the three comparisons in different latitudinal regions.

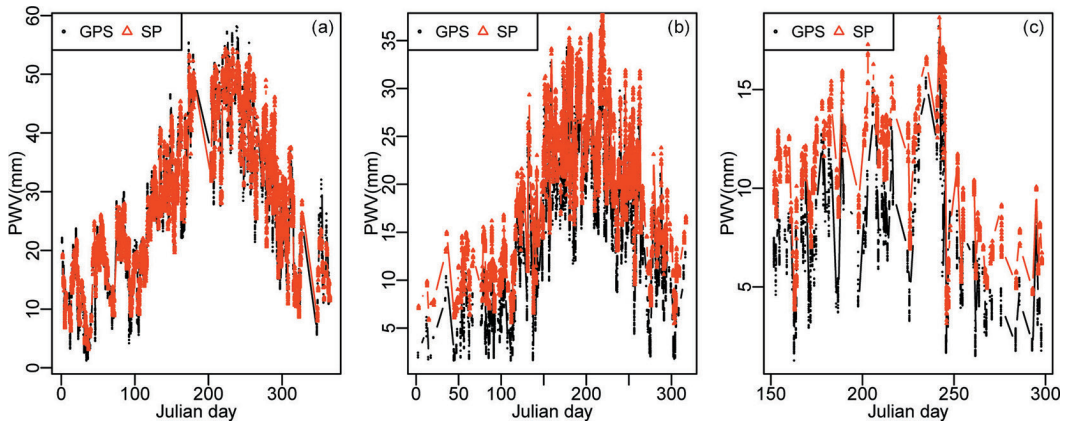


Figure 7: Time series chart of PWV from GPS and Sunphotometer in three latitudinal regions: (a) Tropic, (b) Mid-Latitude and (c) Sub-Arctic.

4 SUMMARY AND CONCLUSIONS

This study first matches the observation stations configured ground-based instruments including radiosonde, GPS receiver and sunphotometer in the globe and in three typical latitudinal climatic regions, then the PWV data from the three instruments are matched each other according to the observing times. After the outliers are removed from the matched data pairs, the multiple PWV comparisons for any two instruments are performed in the globe and in different latitudes. The following conclusions are drawn:

(1) It is found by the multiple PWV comparisons for any two instruments in the globe that the PWV estimates from each instrument show a good consistency with the correlation coefficient above 0.959. The PWV difference of any two instruments displays the normal distribution features, indicating non-systematic biases among the two PWV datasets. The relative differences between sunphotometer and GPS are the smallest, the middle for sunphotometer and radiosonde, and those between GPS and radiosonde are the largest. In general, the radiosonde PWV is overestimated, and sunphotometer PWV is medium, while GPS PWV is underestimated. Hence, the PWV amounts measured by radiosonde are the highest, the middle for sunphotometer, and GPS PWV amounts are the lowest.

(2) The PWV from any two individual instruments has a good agreement in different latitudes, and high correlation coefficients are within the range from 0.915 to 0.989. The PWV mean bias and RMS of any two instruments are always different in the three latitudinal climatic regions; this indicates that latitude and climate have no significant influence on the PWV measurements from three instruments, and that the instruments are very stable and depend on their performance characteristics. The relative differences in different latitudes are the smallest for sunphotometer and GPS, then for sunphotometer and radiosonde, the largest for GPS and radiosonde. As for individual instrument, the highest PWV amounts are still from radiosonde, then for sunphotometer, and the lowest for GPS PWV amounts. Generally, radiosonde is a conventional instrument for observing the upper atmosphere, and it has a long history and near-global coverage over land, but it is usually launched only twice a day. Sunphotometer has high observation frequency while it is limited to work in cloudless and sunny day. GPS receiver has not only high temporal resolution but also is unaffected by bad weather. Hence, GPS PWV is expected to become a promising datum after the amounts are calibrated by the radiosonde PWV.

Acknowledgements

This research was funded jointly by the National Research and Development Program of China (grant number:2020YFA0608203), the National Natural Science Foundation of China (grant number: 41801017), the construction project of weather modification in Northwest China from China Meteorological Administration (grant number: RYSY201907) and the Foundation of Key Laboratory of South China Sea Meteorological Disaster Prevention and Mitigation of Hainan Province, China (grant number: SCSF201909). The authors thank the AERONET and the SOPAC for the data support.

Literature and references:

- Alraddawi, D., Sarkissian, A., Keckhut, P., Bock, O., Noël, S., Beckki, S., Irbah, A., Meftah, M., Claud, C. (2018). Comparison of total water vapour content in the Arctic derived from GNSS, AIRS, MODIS and SCIAMACHY. *Atmospheric Measurement Techniques*, 11, 2949–2965. DOI: <https://doi.org/10.5194/amt-11-2949-2018>
- Bevis M., Businger S., Chiswell S., Herring T. A., Anthes R. A., Rocken C., Ware R. H. (1994). GPS meteorology: Mapping zenith wet delays onto precipitable water. *Journal of applied meteorology*, 33 (3), 379–386. DOI: [https://doi.org/10.1175/1520-0450\(1994\)033<0379:GMMZWD>2.0.CO;2](https://doi.org/10.1175/1520-0450(1994)033<0379:GMMZWD>2.0.CO;2)
- Bevis, M., Businger, S., Herring, T. A., Rocken, C., Anthes, R. A., Ware, R. H. (1992). GPS meteorology: Remote sensing of atmospheric water vapor using the global positioning system. *Journal of Geophysical Research*, 97 (D14), 15787–15801. DOI: <https://doi.org/10.1029/92JD01517>
- Birkenheuer, D., Gutman, S. (2005). A comparison of GOES moisture-derived product and GPS-IPW data during IHOP-2002. *Journal of atmospheric and oceanic technology*, 22, 1838–1845. DOI: <https://doi.org/10.1175/jtech1814.1>
- Bokoye, A. I., Royer, A., Cliche, P., O'Neil, N. (2007). Calibration of sun radiometer-based atmospheric water vapor retrievals using GPS meteorology. *Journal of atmospheric and oceanic technology*, 22, 964–979. DOI: <https://doi.org/10.1175/JTECH2011.1>
- Bruegge, C. J., Conel, J. E., Green, R. O., Margolis, J. S., Holm, R. G., Toon, G. (1992). Water vapor column abundance retrievals during FIFE. *Journal of Geophysical Research*, 97 (D17), 18759–18768. DOI: <https://doi.org/10.1029/92JD01050>
- Campany, E., Bech, J., Rodríguez-Marcos, J., Sola, Y., Lorente, J. (2010). A comparison of total precipitable water measurements from radiosonde and sunphotometers. *Atmospheric Research*, 97, 385–392. DOI: <https://doi.org/10.1016/j.atmosres.2010.04.016>
- Chou, M., Arking, A. (1981). An efficient method for computing the absorption of solar radiation by water vapor. *Journal of the Atmospheric Sciences*, 38, 798–807. DOI: [https://doi.org/10.1175/1520-0469\(1981\)038<0798:aemfct>2.0.co;2](https://doi.org/10.1175/1520-0469(1981)038<0798:aemfct>2.0.co;2)
- Deblonde, G., Macpherson, S., Mireault, Y., Heroux, P. (2005). Evaluation of GPS precipitable water over Canada and the IGS network. *Journal of Applied Meteorology*, 44, 153–166. DOI: <https://doi.org/10.1175/jam-2201.1>
- Dee, D. P., Uppala, S. M., Simmons, A. J., Berrisford, P., Poli, P., Kobayashi, S., Andrae, U., Balmaseda, M. A., Balsamo, G., Bauer, P., Bechtold, P., Beljaars, A. C. M., van de Berg, L., Bidlot, J., Bormann, N., Delsol, C., Dragani, R., Fuentes, M., Geer, A. J., Haimberger, L., Healy, S. B., Hersbach, H., Hólm, E. V., Isaksen, I., Kållberg, P., Köhler, M., Matricardi, M., McNally, A. P., Monge-Sanz, B. M., Morcrette, J.-J., Park, B.-K., Peubey, C., de Rosnay, P., Tavolato, C., Thépaut, J.-N., Vitart, F. (2011). The ERA-Interim reanalysis: configuration and performance of the data assimilation system. *Quarterly Journal of the Royal Meteorological Society*, 137, 553–597. DOI: <https://doi.org/10.1002/qj.828>
- Duan, J., Bevis, M., Fang, P., Bock, Y., Chiswell, S., Businger, S., Rocken, C., Solheim,

- F., Hove, T. V., Ware, R., McClusky, S., Herring, T. A., King, R. W. (1996). GPS Meteorology: Direct estimation of the absolute value of precipitable water. *Journal of Applied Meteorology*, 35, 830–838. DOI: [https://doi.org/10.1175/1520-0450\(1996\)035<0830:gmdetot>2.0.co;2](https://doi.org/10.1175/1520-0450(1996)035<0830:gmdetot>2.0.co;2)
- Elgered, G., Davis, J. L., Herring, T. A., Shapiro, I. I. (1991). Geodesy by radio interferometry: Water vapor radiometry of estimation of the wet delay. *Journal of Geophysical Research*, 96, 6541–6555. DOI: <https://doi.org/10.1029/90JB00834>
- Giles, D. M., Sinyuk, A., Sorokin, M. G., Schafer, J. S., Smirnov, A., Slutsker, I., Eck, T. F., Holben, B. N., Campbell, J. R., Welton, E. J., Korkin, S. V., Lyapustin, A. I. (2019). Advancements in the Aerosol Robotic Network (AERONET) Version 3 database – automated near-real-time quality control algorithm with improved cloud screening for Sun photometer aerosol optical depth (AOD) measurements. *Atmospheric Measurement Techniques*, 12, 169–209. DOI: <https://doi.org/10.5194/amt-12-169-2019>
- Gong, S. (2018). Evaluation of Maritime Aerosol Optical Thickness and Precipitable Water Vapor Content from the Microtops II Sun Photometer. *Optik*, 169, 1–7. DOI: <https://doi.org/10.1016/j.ijleo.2018.05.025>
- Gulstad, L., Isaksen, I. S. A. (2007). Modeling Water Vapor in the Upper Troposphere and Lower Stratosphere. *Terrestrial, Atmospheric and Oceanic Sciences*, 18 (3), 415–436. DOI: [https://doi.org/10.3319/TAO.2007.18.3.415\(EA\)](https://doi.org/10.3319/TAO.2007.18.3.415(EA))
- Halthore, R., Eck, T., Holben, B., Markham, B. (1997). Sun photometric measurements of atmospheric water vapour column abundance in the 940nm band. *Journal of Geophysical Research*, 102 (D4), 4343–4352. DOI: <https://doi.org/10.1029/96jd03247>
- Holben, B., Eck, T., Slutsker, I., Tanré, D., Buis, J., Setzer, A., Vermote, E., Reagan, J., Kaufman, Y., Nakajima, T., Lavenue, F., Jankowiak, I., Smirnov, A. (1998). AERONET—a federated instrument network and data archive for aerosol characterization. *Remote Sensing of Environment*, 66, 1–16. DOI: [https://doi.org/10.1016/S0034-4257\(98\)00031-5](https://doi.org/10.1016/S0034-4257(98)00031-5)
- Iwabuchi, T., Naito, I., Mannoji, N. (2000). A comparison of global positioning system retrieved precipitable water vapor with the numerical weather prediction analysis data over the Japanese Islands. *Journal of geophysical research*, 105 (D4), 4573–4585. DOI: <https://doi.org/10.1029/1999JD901007>
- Jade, S., Vijayan M. S. M., Gaur V. K., Prabhu T. P., Sahu S. C. (2005). Estimates of precipitable water vapour from GPS data over the Indian subcontinent. *Journal of Atmospheric and Solar-Terrestrial Physics*, 67, 623–635. DOI: <https://doi.org/10.1016/j.jastp.2004.12.010>
- Kuo, Y., Schreiner, W. S., Wang, J., Rossiter, D. L., Zhang, Y. (2005). Comparison of GPS radio occultation soundings with radiosondes. *Geophysical Research Letters*, 32 (L05817). DOI: <https://doi.org/10.1029/2004GL021443>
- Li, Z., Muller J., Cross P. (2003). Comparison of precipitable water vapor derived from radiosonde, GPS, and Moderate-Resolution Imaging Spectroradiometer measurements. *Journal of Geophysical Research*, 108 (D204651), DOI: <https://doi.org/10.1029/2003jd003372>
- Liu, H., Tang, S., Zhang, S., Hu, J. (2015). Evaluation of MODIS water vapour products over China using radiosonde data. *International Journal of Remote Sensing*, 36 (2), 680–690. DOI: <https://doi.org/10.1080/01431161.2014.999884>
- Liu, H., Wang, Y., Wang, J., Li, J., Cao, X., Xiong, B. (2009). Preliminary analysis of the characteristics of precipitable water vapor measured by the ground-based 12-channel microwave radiometer in Beijing. *Chinese Journal of Atmospheric Sciences*, 33 (2), 388–396.
- Liou, K. N. (2002). *An introduction to atmospheric radiation*. Florida: Academic Press.
- Lu, C., Li, X., Ge, M., Heinkelmann, R., Nilsson, T., Soja, B., Dick, G., Schuh, H. (2016). Estimation and evaluation of real-time precipitable water vapor from GLONASS and GPS. *GPS Solution*, 20, 703–713. DOI: <https://doi.org/10.1007/s10291-015-0479-8>
- Mockler, S. B. (1995). *Water vapor in the climate system*. Special report, AGU, Washington D. C.
- Morys, M., Mims III, F. M., Hagerup, S., Anderson, S. E., Baker, A., Kia, J., Walkup, T. (2001). Design, calibration, and performance of MICROTOPS II handheld ozone monitor and Sun photometer. *Journal of Geophysical Research*, 106, 14573–14582. DOI: <https://doi.org/10.1029/2001jd900103>
- Ohtani, R., Naito, I. (2000). Comparisons of GPS-derived precipitable water vapors with radiosonde observations in Japan. *Journal of Geophysical Research*, 105 (D22), 26917–26929. DOI: <https://doi.org/10.1029/2000jd900362>
- Robert, K., Kalnay, E., Collins, W., Saha, S., White, G., Woollen, J., Chelliah, M., Ebisuzaki, W., Kanamitsu, M., Kousky, V., Dool, H., Jenne, R., Fiorino, M. (2001). *The NCEP–NCAR 50-Year Reanalysis: Monthly Means CD-ROM and Documentation*. *Bulletin of the American Meteorological Society*, 82 (2), 247–268. DOI: [https://doi.org/10.1175/1520-0477\(2001\)082<0247:tnnyrm>2.3.co;2](https://doi.org/10.1175/1520-0477(2001)082<0247:tnnyrm>2.3.co;2)
- Senica, A., Sterle O., Pavlovič Prešeren, P. (2018). Določitev vpliva troposfere na opazovanje GNSS iz niza radiosondaznih meritev v Ljubljani od oktobra do decembra 2017. *Geodetski vestnik*, 62 (3), 415–429. DOI: <https://doi.org/10.15292/geodetski-vestnik.2018.03.415-429>
- Shi, F., Xin, J., Yang, L., Cong, Z., Liu, R., Ma, Y., Wang, Y., Lu, X., Zhao, L. (2018). The first validation of the precipitable water vapor of multi-sensor satellites over the typical regions in China. *Remote Sensing of Environment*, 206, 107–122. DOI: <https://doi.org/10.1016/j.rse.2017.12.022>
- Shi, J., Xu, C., Guo, J., Gao, Y. (2015). Real-time GPS precise point positioning-based precipitable water vapor estimation for rainfall monitoring and forecasting. *IEEE transactions on geoscience and remote sensing*, 53 (6), 3452–3459. DOI: <https://doi.org/10.1109/tgrs.2014.2377041>
- Smirnov, A., Holben, B. N., Slutsker, I., Giles, D. M., McClain, C. R., Eck, T. F., Sakerin, S. M., Macke, A., Croot, P., Zibordi, G., Quinn, P. K., Sciare, J., Kinne, S., Harvey, M., Smyth, T. J., Piketh, S., Zielinski, T., Proshutinsky, A., Goes, J. I., Nelson, N. B., Larouche, P., Radionov, V. F., Goloub, P., Moorthy, K. K., Matarrese, R., Robertson, E. J., Jourdin, F. (2009). Maritime Aerosol Network as a component of Aerosol Robotic Network. *Journal of Geophysical Research*, 114 (D06204). DOI: <https://doi.org/10.1029/2008JD011257>
- Soe, H., Gilerson, A., Foster, R., Wang, M., Arnore, R., Ahmed, S. (2014). Radiometric calibration of ocean color satellite sensors using AERONET-OC data. *Optics Express*, 22 (19), 23385–23401. DOI: <https://doi.org/10.1364/oe.22.023385>
- Tregoning, P., Reinout, B., Denis O'Brien, Martin, H. (1998). Accuracy of absolute precipitable water vapor estimates from GPS observations. *Journal of Geophysical Research*, 103 (D22), 28701–28710. DOI: <https://doi.org/10.1029/98jd02516>
- UCSD. (2002). *SOPAC/CSRC Garner GPS Archive*, <http://garner.ucsd.edu/>

- Vaquero-Martínez, J., Antón, M., Galisteo, J. P. O., Cachorro, V. E., Álvarez-Zapatero, P., Román, R., Loyola, D., Costa, M. J., Wang, H., Abad, G. G., Noël, S. (2018). Inter-comparison of integrated water vapor from satellite instruments using reference GPS data at the Iberian Peninsula. *Remote Sensing of Environment*, 204, 729–740. DOI: <https://doi.org/10.1016/j.rse.2017.09.028>.
- Vaquero-Martínez, J., Antón, M., Galisteo, J. P. O., Cachorro, V. E., Costa, M. J., Román, R., Bennouna, Y. S. (2017). Validation of MODIS integrated water vapor product against reference GPS data at the Iberian Peninsula. *International Journal of Applied Earth Observation and Geoinformation*, 63, 214–221. DOI: <http://doi.org/10.1016/j.jag.2017.07.008>
- Vijayakumar, K., Devara, P. C. S., Giles, D. M., Holben, B. N., Rao, S. V. B., Jayasankar, C. K. (2018). Validation of satellite and model aerosol optical depth and precipitable water vapour observations with AERONET data over Pune, India. *International Journal of Remote Sensing*, 39 (21), 7643–7663. DOI: <https://doi.org/10.1080/01431161.2018.1476789>
- Wang, B., Liu, G. (1993). An estimation of total atmospheric water vapor in the mainland of China. *Acta Geographica Sinica*, 48 (3), 244–253.
- Wang, J., Zhang, L., Dai, A., Hove, T. V., Baelen, J. V. (2007). A near-global, 2-hourly data set of atmospheric precipitable water from ground-based GPS measurements. *Journal of Geophysical Research*, 112(D11107). DOI: <https://doi.org/10.1029/2006JD007529>
- Wang, M., Fang, X., Hu, S., Hu, H., Li, T., Dou, X. (2015). Variation characteristics of water vapor distribution during 2000–2008 over Hefei (31.9°N, 117.2°E) observed by L625 lidar. *Atmospheric Research*, 164–165. DOI: <https://doi.org/10.1016/j.atmosres.2015.04.003>
- Wang, J., Zhang, L., Dai, A. (2005). Global estimates of water-vapor-weighted mean temperature of the atmosphere for GPS applications. *Journal of Geophysical Research*, 110 (D21101). DOI: <https://doi.org/10.1029/2005JD006215>
- Ware, R., Exner, M., Feng, D., Gorbunov, M., Hardy, K., Herman, B., Kuo, Y., Meehan, T., Melbourne, W., Rocken, C., Schreiner, W., Sokolovskiy, S., Solheim, F., Zou, X., Anthes, R., Businger, S., Trenberth, K. (1996). GPS sounding of the atmosphere from low earth orbit: preliminary results. *Bulletin of the American Meteorological Society*, 77 (1), 19–40. DOI: [https://doi.org/10.1175/1520-0477\(1996\)077<0019:gsotaf>2.0.co;2](https://doi.org/10.1175/1520-0477(1996)077<0019:gsotaf>2.0.co;2)
- WMO. (2008). *Guide to Meteorological Instruments and Methods of Observation*. EOSTransactions, 8, 1–681.
- Xu, X., Luo, J., Shi, C. (2009). Comparison of COSMIC radio occultation refractivity profiles with radiosonde measurements. *Advances in Atmospheric Sciences*, 26 (6), 1137–1145. DOI: <https://doi.org/10.1007/s00376-009-8066-y>
- Zeng, Z., Mao, F., Wang, Z., Guo, J., Gui, K., An, J., Yim, S. H. L., Yang, Y., Zhang, B., Jiang, H. (2019). Preliminary Evaluation of the Atmospheric Infrared Sounder Water Vapor over China Against High-Resolution Radiosonde Measurements. *Journal of Geophysical Research: Atmospheres*, 124, 3871–3888. DOI: <https://doi.org/10.1029/2018JD029109>.
- Zhai, P., Eskridge, R. (1997). Atmospheric water vapor over China. *Journal of Climate*, 10 (10), 2643–2652. DOI: [https://doi.org/10.1175/1520-0442\(1997\)10<2643:AWVOC>2.0.CO;2](https://doi.org/10.1175/1520-0442(1997)10<2643:AWVOC>2.0.CO;2)
- Zibordi, G., Holben, B., Slutsker, I., Giles, D., D'Alimonte, D., Mélin, F., Berthon, J., Vandemark, D., Feng, H., Schuster, G., Fabbri, B. E., Kaitala, S., Seppälä, J. (2009). AERONET-OC: A Network for the Validation of Ocean Color Primary Products. *Journal of Atmospheric and Oceanic Technology*, 26 (8), 1634–1651. DOI: <https://doi.org/10.1175/2009JTECH0654.1>



Gong S., Chen W., Zhang C., Wu P., Han J. (2020). Intercomparisons of precipitable water vapour derived from radiosonde, GPS and sunphotometer observations. *Geodetski vestnik*, 64 (4), 562–577. DOI: <https://doi.org/10.15292/geodetski-vestnik.2020.04.562-577>

Shaoqi Gong

*Nanjing University of Information Science & Technology
School of Remote Sensing and Geomatics Engineering
Nanjing, 210044, China and
Key Laboratory of South China Sea Meteorological Disaster
Prevention and Mitigation of Hainan Province, Sanya, 570203,
China; National Climate Center, China Meteorological Admini-
stration, Beijing, 100081, China
e-mail: shaoqigong@163.com*

Wenqian Chen

*Nanjing University of Information Science & Technology
School of Remote Sensing and Geomatics Engineering
Nanjing, 210044, China
e-mail: wenqchen@163.com*

Prof. Cunjie Zhang*

*National Climate Center, China Meteorological Administration
and Key laboratory for Cloud Physics of China Meteorological
Administration, Beijing, 100081, China)
Beijing, 100081, China
e-mail: zhangcj@cma.gov.cn
Corresponding author

Ping Wu

*National Climate Center, China Meteorological Administration
Beijing, 100081, China
e-mail: wup@cma.gov.cn*

Jing Han

*Key Laboratory of South China Sea Meteorological Disaster
Prevention and Mitigation of Hainan Province
Sanya, 570203, China
e-mail: hanjing8361@163.com*